HHS Public Access

Author manuscript

Nat Neurosci. Author manuscript; available in PMC 2013 July 03.

Published in final edited form as:

Nat Neurosci. 2013 January ; 16(1): 64–70. doi:10.1038/nn.3269.

Closed-loop optogenetic control of thalamus as a new tool to interrupt seizures after cortical injury

Jeanne T. Paz[1], **Thomas J. Davidson**[2], **Eric S. Frechette**[1], **Bruno Delord**[3], **Isabel Parada**[1], **Kathy Peng**[1], **Karl Deisseroth**[2], and **John R. Huguenard**[1]

[1]Department of Neurology and Neurological Sciences, Stanford University School of Medicine, Stanford, CA 94305, USA

[2]Department of Bioengineering, Stanford University School of Medicine, Stanford, CA, 94305, USA

[3]Institut des Systèmes Intelligents et de Robotique, CNRS – UMR 7222, Université Pierre et Marie Curie, Paris, France

Abstract

Cerebrocortical injuries, such as stroke, are a major source of disability. Maladaptive consequences can result from post-injury local reorganization of cortical circuits. For example, epilepsy is a common sequela of cortical stroke, yet mechanisms responsible for seizures following cortical injuries remain unknown. In addition to local reorganization, long-range, extra-cortical connections might be critical for seizure maintenance. Here we report in rats the first evidence that the thalamus – a structure remote from but connected to the injured cortex – is required to maintain cortical seizures. Thalamocortical neurons connected to the injured epileptic cortex undergo changes in HCN channel expression and become hyperexcitable. Targeting these neurons with a closed-loop optogenetic strategy demonstrates that reducing their activity in real-time is sufficient to immediately interrupt electrographic and behavioral seizures. This approach is of therapeutic interest for intractable epilepsy, since it spares cortical function between seizures, in contrast to existing treatments such as surgical lesioning or drugs.

INTRODUCTION

Despite the high prevalence of stroke and epilepsy – both major sources of disability[1,2,3,4], – the underlying cellular and circuit mechanisms leading from stroke to epilepsy remain unknown and often injury-induced epilepsies do not respond to existing treatments[3,5]. It is important to identify the neural circuits involved in injury-induced epilepsy to pinpoint the exact nature of the causally important alterations in these circuits and to control seizures with specific interventions.

Corresponding authors: john.huguenard@stanford.edu and jtpaz@stanford.edu.

Author contributions: JTP and JRH designed the experiments and wrote the manuscript; JTP performed all *in vitro* experiments; JTP and TJD designed and performed *in vivo* experiments; BD performed computational modeling; KP performed pilot EEG recordings; IP performed histology; JTP, JRH, ESF analyzed data. KD provided reagents/tools.

Although altered short-range cortical circuit function is thought to be the primary cause of injury-induced epilepsies[6–7], the additional role of long-range connections to and from injured cortex to other brain regions in seizure maintenance has not been adequately studied. The cortex is intimately connected with thalamus and the cortico-thalamo-cortical excitatory loop mediates network oscillations underlying epilepsies in man and in animal models[8]. Yet, despite pioneering studies demonstrating the recruitment of thalamus in cortical seizures[8,9,10,11,12,13], its role in seizure expression, especially in acquired epilepsies, remains unknown. The thalamus is composed of both excitatory and inhibitory neurons; and adjacent corticothalamic and thalamocortical glutamatergic axons; therefore it is challenging to selectively activate thalamocortical or corticothalamic axons and it is impossible to control their activity in real-time using traditional pharmacological or electrical manipulations. Here we overcame this challenge by using optogenetic methods[14] that allow for control of a specific cell type with high temporal precision. While recent studies have used optogenetic tools to study seizure-like activities *in vitro*[15,16], an interrogation of the causal relationship between activity of one cell type and the seizure and its disruption in real-time has never been tested in behaving animals.

The peri-infarct cortex is generally considered to be the zone where seizures initiate[6–7], yet the extent of cortical damage precludes effective antiepileptic targeting of the entire peri-infarct hyperexcitable cortex. In addition, targeting of such extensive areas might disrupt function of eloquent cortex. The scope of this study was to determine, independent of where seizures initiate, whether a) the secondarily damaged thalamus was required to sustain post-stroke seizures, and b) if so, whether this focal region could be readily targeted to stop seizures.

We induced focal cortical strokes and first located and delineated potentially epileptic cellular and circuit changes in thalamus *in vitro*. We then engineered an approach to specifically inhibit output from that thalamic region to test whether it is causally involved in seizure maintenance *in vivo*. For this purpose, we used an established model of cortical photothrombosis that results in late epilepsy (>1month) after stroke[17,18]. This injury is associated with reduced excitability and excitation in the inhibitory reticular thalamic (RT) neurons and retrograde cell death and gliosis specifically in ipsilateral ventroposterolateral thalamic nucleus (VPL); these changes are known to be complete by the end of the first week and are sustained over months[19] (Supplemental Fig. 1a,b).

RESULTS

Cortical stroke enhances intrinsic excitability of TC cells

Seven to fourteen days following focal cortical stroke, ipsilateral thalamocortical (TC) neurons showed an increased membrane intrinsic excitability and enhanced rhythmogenic properties. Specifically, TC cells showed an increased input resistance resulting from a reduced membrane area (Fig. 1a–e), and a slightly depolarized resting membrane potential (not shown). In agreement with the increased input resistance after injury, rheobase was reduced, while properties of individual action potentials were not altered (Supplemental Table 1). Affected TC cells demonstrated several alterations in the biophysical properties of hyperpolarization-activated cyclic nucleotide-gated (HCN) channel-mediated current (Ih,

Fig 2): faster activation and a depolarized half-activation voltage ($V_{50\%}$), no change in Ih density, and a reduced responsiveness of Ih to cAMP (not shown)..Changes in Ih result in part from enhanced constitutive cAMP signaling (not shown) and a switch in predominant HCN subunits (Supplemental Fig. 2). Notably, similar changes in Ih have been also linked to genetic epilepsies (for review see [20]).

The increased intrinsic excitability was robust in cells close to the injured gliotic area (medial VPL, lateral VPM) but was not significant in thalamic areas not affected by cell death or gliosis, e.g. medial VPM or VL (Fig. 1 a–c, e). Notably, the changes in intrinsic excitability started within the first week after stroke, before seizures, and persisted into the chronic post-stroke epileptic state (>1 month) suggesting that these changes do not represent a transient, preapoptotic phenomenon.

Cortical stroke leads to epileptiform thalamic oscillations

We next asked whether the increased TC intrinsic excitability translated into altered circuit function within the thalamus. For this purpose, we assessed thalamic network activity in horizontal thalamic slices using multiunit extracellular recordings 7–14 days post-stroke. Such slices conserve intra-thalamic connectivity between nRT and TC nuclei, but not with cortex[21]. In slices from control animals, electrical stimulation of the internal capsule evoked rhythmic activity in thalamus, in agreement with previous findings (Fig. 3a)[15,22,23]. The duration of the evoked activity was increased in slices from injured rats (Fig. 3a).

In addition to enhanced evoked oscillations, post-stroke (“injured”) thalamic slices (8 of 8 slices from 3 rats) also generated 1–5 s – long robust spontaneous epileptiform network oscillations that were never observed in control slices (0 of 5 slices from 3 rats) (Fig. 3a). This epileptiform activity was observed in the gliotic thalamus and within ~200 μm of its border, corresponding to the border between VPL and VPM, including the lateral VPM. These results indicate that cortical stroke leads over time to a hyperexcitable intra-thalamic network of surviving cells that is then able to generate epileptiform activities. Similar multiunit bursting activity in thalamus was observed during spontaneously occurring seizures in awake, behaving rats post-stroke (see Supplemental movie 1).

Computational modelling of intrathalamic network activity

We assessed whether TC cellular modifications could be responsible for enhanced oscillations in the thalamic network in a computational model including TC and nRT neurons and a constant cortical input (Fig. 3b, top). We first demonstrated in a single-cell model that the combined modifications in membrane area and in Ih (depolarized half-activation voltage ($V_{50\%}$) and faster activation time constant (τ_a)) account for the post-stroke hyperexcitability in TC cells (Supplemental Fig. 3). We found that these intrinsic changes in cell size and in Ih activation properties enhance thalamic network oscillations (Fig. 3b bottom, c; Supplemental Fig. 4). Specifically, a change in both intrinsic properties reduced the threshold for initiation of oscillations, as it increased the magnitude of the hyperpolarizing current required to prevent the oscillation (Fig. 3c). Notably, this effect on threshold resulted from a supra-linear interaction of intrinsic changes (Fig. 3d).

Moreover, the oscillation duration was enhanced by the changes in intrinsic excitability in TC neurons (Fig. 3e, top, and Supplemental Fig. 5). Thus, the alterations we found in Ih and in membrane area in injured TC cells (Figs.1 and 2) are "epileptic" in that they make the thalamus oscillate for longer durations or in conditions in which it would normally be silent. The enhanced oscillations in the injured conditions were very robust in that they were unaffected by reducing nRT spike output (not shown), which would result from reduced excitability of nRT following focal cortical stroke[19]. Finally, we found that we were able to restore both the duration and the threshold of oscillation initiation by modifying h and leak conductances, g_h and g_L, respectively (Fig. 3d, e bottom; Supplemental Figs. 4 and 5).

Cortical stroke induces thalamocortical epilepsy

Chronic monitoring of control (n=7) and injured (n=5) animals up to 10 months revealed that stroke resulted in spontaneous ictal activity only in injured rats (3 out of 5). Seizures were 10–120 s–long and occurred >1 month post-stroke in agreement with previous studies[17,18,24] and were associated with a motor arrest (Supplemental Movies 2, 3). The oscillatory power of the ictal EEG peaked in the 3–5 Hz and 8–10 Hz frequency bands (Figs. 4c; Supplemental Fig. 6c) and had a different spectral signature than typical absence seizures in rats, in agreement with [17].

Post-stroke seizures had clear thalamic involvement even though their spectral properties were distinct from typical thalamocortical absence seizures. Also, seizure-like oscillations usually spread to the contralateral hemisphere in agreement with [24] and were synchronized in cortical EEG and thalamic local field potentials (LFPs) (Figs. 4a,b, and 5c; Supplemental Figs. 6a,b and 7d).

Optical TC inhibition ends seizures in awake behaving rats

Next we asked whether TC cell activity is important for seizure expression *in vivo*. To test whether seizures could be terminated by selectively inhibiting TC neurons, we transduced either eNpHR3.0, which enables membrane hyperpolarization and reduction of action potential firing when illuminated with yellow light[25], or eYFP alone, under the Camk2α promoter, in the ventrobasal (VB) thalamus ipsilateral to cortical stroke. Next, we designed a device containing multiple EEG electrodes and a chronic multi-site optrode[26] (CMO, Supplemental Fig. 7b; see Methods). We implanted the CMO in ipsilateral VB thalamus (Fig. 5a) to allow a selective illumination of TC neurons while monitoring their firing. We also implanted four chronic EEG electrodes, two above peri-stroke cortex (within ~0.5 mm from the edge of lesion) and two in the corresponding contralateral cortex (Supplemental Fig. 8c and Methods). This allowed us to monitor the effect of optical inhibition of TC neurons on simultaneously recorded TC multiunit firing and LFP, cortical EEG, and behavior in 4 rats. Selective illumination of eNpHR3.0-expressing TC neurons with 594 nm light interrupted ongoing electrographic epileptic activities in thalamus and cortex (Fig. 5c, d *left*) as well as the behavioral seizure, and the animals immediately resumed normal behavior (Supplemental movie 4). The finding that inhibition of TC neurons ipsilateral to stroke interrupted not only ipsilateral but also contralateral seizures indicates that seizures were generated in the hemisphere ipsilateral to stroke. Upon interruption of the seizure by light, there was a resumption of normal thalamic and cortical activities (Fig. 5c,e,f)

coinciding with a switch to a non-epileptic behavior. In sum, selectively inhibiting TC output was sufficient to *switch off* the ongoing electrographic and behavioral seizure.

Lower intensity light (≤5 mW) did not significantly affect thalamic activity and was not effective in disrupting seizures (Supplemental Fig. 7a,c,d). Notably, the laser light at the intensity used to silence the seizures did not affect normal physiological rhythms in control non-injured animals (not shown) or the normal EEG activities between seizures (referred to as interictal in the manuscript) in epileptic animals (Fig. 5e,d *right*, Supplemental Fig. 8a right) and did not seem to affect normal interictal behavior such as sleep (Supplemental movie 5).

In contrast to eNpHR3.0-transduced animals, light had no effect in eYFP-transduced animals, indicating that disruption of thalamocortical oscillations and seizures was due to eNpHR3.0 activation and not to non-specific effects of light, such as heating, or visual cueing. We also confirmed that 594 nm light illumination silenced the firing of eNpHR3.0-expressing TC neurons *in vitro* (n=9 cells from 4 rats; Supplemental Fig. 9) and reduced the multiunit firing in the thalamus in eNpHR3.0-transduced (n=4 rats: 2 injured and 2 non-injured) but not in eYFP-transduced behaving animals (n=2 injured rats; Fig. 6).

Finally, we engineered a novel method to detect and silence seizures online in chronically implanted rats (Supplemental Fig. 1c). An EEG channel was routed to a real-time processor that calculated the EEG line-length[27] and triggered laser stimulation upon crossing of a threshold. This system was capable of detecting and silencing seizures within 1 second of initiation (Figs. 7 and 8; Supplemental Fig. 1; Supplemental movies 6 and 7). We were able to validate this method up to nearly a year post-stroke in 2 injured rats with chronic implants (Figs. 7 and 8; Supplemental Figs. 1c and 8).

DISCUSSION

Here, we used temporally precise, cell-type-specific optogenetic manipulations, to identify a neural substrate that can be readily targeted for post-injury seizure control. In sum, we found that focal photothrombotic stroke in the rat somatosensory cortex leads to secondary changes and hyperexcitability in the functionally related thalamus. Changes in input resistance and in Ih in TC neurons enhance their rhythmogenesis. A minimal computational model indicated such changes increase thalamic network excitability and support epileptiform oscillations. To test this model, we designed a method to specifically silence TC neurons from this hyperexcitable thalamic region in real-time. Reducing the thalamocortical output rapidly (<1s) interrupted the electrographic and behavioral seizure. Thus, we provide the first evidence that TC neuronal activity is required for post-stroke epilepsy given that reducing TC activity is *sufficient* to disrupt seizures either at their onset or after their generalization. The finding of remarkable efficacy of thalamic inhibition was not expected in light of the current working model, according to which epilepsy results mainly from maladaptive reorganization in cortex adjacent to the damaged area. Disruption of seizures at their onset with closed-loop control, *via* a brief targeted inhibition of TC cells, as we have demonstrated here, is a promising potential therapeutic approach for otherwise untreatable epilepsies, since it would not affect normal brain activity between seizures, as

might other therapeutic approaches such as surgical lesions, or chronic treatment with pharmacological agents.

It is important to note that the goal of our study was *not* to determine the exact site of seizure initiation. Irrespective of the question of whether the seizure initiates in cortex or thalamus, here we demonstrate that the thalamic output is required to *maintain* the cortical electrographic and behavioral seizure. A major advantage of targeting thalamocortical *maintenance* of seizures is that this novel mechanism of a rapid disruption of seizures *via* a brief inhibition of thalamus would be synergistic with other treatments targeting, for example, seizure initiation, seizure spread or secondary epileptogenesis. Another key benefit of targeting thalamus is that it would not disrupt higher cognitive functions dependent on intracortical processing.

The Ih alterations we observed in TC cells are similar to what has been described in other epilepsy models[20] suggesting that these alterations could be a mechanism common to various epilepsies. The finding of altered intrinsic properties (Ih and Rin) in TC neurons that enhance rhythmogenesis led us to hypothesize and demonstrate that inhibiting these hyperexcitable TC neurons could rapidly abort cortical seizures.

Even though Ih alterations do not entirely account for thalamic hyperexcitability, it is possible that manipulating Ih, either chronically or transiently, could also lead to seizure disruption. Indeed, as suggested by our computational model, combining a reduction in g_h and increase in g_L in TC cells is expected to be anti-epileptic. However for real time anti-seizure control we chose a cell-type specific optogenetic approach rather than a pharmacological manipulation of Ih. The latter would neither be cell specific nor provide real time control. Future technologies might allow targeted real time manipulation of ion channel mediated currents such as I_h that might be as effective and more specific treatments of the epileptic injury. Alternatively, the broad but temporally-specific reduction of thalamocortical excitability that we have demonstrated here may prove the most effective approach.

In conclusion, our findings at cellular, network and behavioral levels provide causal support for the hypothesis that the thalamus is critically involved in cortical injury-induced epilepsy and also lead to a novel general concept that a structure remote from but connected to primary damaged tissue *via* long-range projections can be critically involved in abnormal brain activity such as seizures. Our results suggest novel roles for long-range connections in maintaining normal and pathologic oscillations, and also suggest potential future novel therapeutic strategies of silencing specific remote structures in cases where removal of the damaged cortical area is not an option or does not result in seizure control. The finding that thalamus is critical for maintaining seizure activity suggests that targeting a spatially restricted region of the thalamus might be a more tractable therapeutic target for neural modulation than targeting the corresponding, yet more spatially extended, cortical abnormality.

METHODS

We performed all of the experiments according to protocols approved by the Stanford Institutional Animal Care and Use Committee, and every precaution was taken to minimize stress and the number of animals used in each series of experiments.

Cortical photothrombotic stroke

We performed photothrombosis as described[19] on Sprague Dawley rats on postnatal days 25–30, P25–30. Briefly, we anesthetized the rats, injected the light sensitive Rose Bengal dye (40 mg/kg) (Sigma-Aldrich) into the tail vein and focused on the skull a light from a 3-mm-diameter fiber optic cable. The optical system was designed to have an emission spectrum that encompassed the *in vivo* absorption range of Rose Bengal (maximum absorbance at 562 nm). To induce a focal photothrombotic lesion in the right somatosensory cortex we centered the light beam 4.5 – 5 mm lateral and 2.5 mm caudal to bregma. Control littermate rats received the same injection of Rose Bengal but were not photostimulated.

Slice preparation

We anesthetized injured and control littermate rats (postnatal day 30–180, P30–180) with pentobarbital (100 mg per kg, intraperitoneal) and decapitated them. We prepared thalamic slices as previously described[15].

Thalamic oscillations

We recorded extracellular multiunit activity in horizontal slices (400 μm) containing somatosensory thalamus as described[15]. Briefly, we placed thalamic slices in an interface chamber at 34 °C and superfused at a rate of 2 $ml.min^{-1}$ with oxygenated artificial cerebrospinal fluid (ACSF) containing 126 mM NaCl, 2.5 mM KCl, 1.25 mM NaH_2PO_4, 2 mM $MgCl_2$, 2 mM $CaCl_2$, 26 mM $NaHCO_3$ and 10 mM glucose, equilibrated with 95% O_2 and 5% CO_2, pH 7.4, supplemented with 0.3 mM glutamine[23]. We performed extracellular multiunit recordings with monopolar tungsten microelectrodes (50–100 kΩ, FHC) placed in VB thalamus. Signals were amplified 10,000 times and band-pass filtered between 100 Hz and 3 kHz. We delivered electrical stimuli to the internal capsule with a pair of tungsten microelectrodes (50–100 kΩ, FHC). The stimuli were 100 μs in duration, 50 V in amplitude, and delivered once every 30 s.

Whole-cell patch-clamp electrophysiology from thalamic slices

We performed the recordings as previously described[15]. We visually identified nRT and TC neurons using differential contrast optics with a Zeiss (Oberkochen) Axioskop microscope and an infrared video camera. Recording electrodes made of borosilicate glass had a resistance of 2.5–4 MΩ when filled with intracellular solution. During recordings we filled the cells with 0.2–0.5% biocytin (Sigma-Aldrich) included in the internal solution. We corrected the potentials for −15–mV liquid junction potential. We performed the recordings in presence of $GABA_A$ receptor antagonist picrotoxin (50 μM, Tocris). We blocked $GABA_A$ receptors to determine whether the increased input resistance of TC neurons in injured versus control rats resulted from changes in $GABA_A$ receptor–mediated conductance which we suspected, given that the inhibitory RT–TC pathway is dramatically reduced after

stroke[19]. We monitored the access resistance in all the recordings, and we included cells for analysis only if the access resistance was <18 MΩ and the change of resistance was <20% over the course of the experiment. We fixed whole slices and processed them using the standard avidin–biotin peroxidase method (Horikawa and Armstrong, 1988; Tseng et al., 1991). We processed the slices for immunofluorescence for glial fibrillary acidic protein (GFAP) (Millipore)[19]. We assessed immunofluorescence with a laser confocal microscope (Zeiss LSM 510).

Ih activation and de-activation curves[28]

Ih activation curve[28]—The Ih activation curve was constructed by measuring tail currents elicited by repolarizing the membrane to −65mV holding level following voltage-steps between −60 to −135mV (Fig. 2a,c). We measured Ih at the tail current 0.7s after the test voltage pulse (see arrowheads in Fig. 2a) to minimize the contribution of capacitative or non-Ih active currents by allowing sufficient time for these events to dissipate before measuring Ih[28]. We normalized the tail current amplitudes (Itail) to the maximal amplitude (Itail max) and plotted against the membrane potential to which the neuron was stepped during activation of Ih (Fig. 2a). The resulting data were then fitted with a Boltzmann function:

$$I/I_{max} = (A1 - A2)/(1 + e^{(V - V50\%)/k}) + A2$$

where $V_{50\%}$ and k represent the half-maximal voltage and Boltzmann slope factor, respectively; $A1$ and $A2$ represent initial and final I/I_{max} values, respectively.

Ih activation and de-activation time constants—Over the entire voltage range tested, Ih was well fitted (r=0.99) by a single-exponential function:

$I(t) = A_0 + A_1\, e^{-t/\tau}$ where $I(t)$ is the amplitude current at time t, A_0 and A_1 are amplitude components, and τ is the time constant (Fig. 2f,g).

Ih de-activation curves were performed as explained in Fig. 2

Patch clamp electrophysiology data acquisition and analysis—We used Digidata 1320 digitizer and pClamp9 (Molecular Devices) for data aquisition and analysis. We amplified the signals with Multiclamp 700a (Molecular Devices), and sampled and filtered them at 10 kHz. We calculated the amplitude of action potentials as the potential difference between their voltage threshold and the peak of the waveform.

Experimental design and statistical analysis—Numerical values are given as means ± s.e.m. unless stated otherwise. The sample sizes used in this report are standard for the field. For statistical analyses, we assessed normality (Sigmastat) before choosing the relevant comparative test. We used non parametric tests in cases where the normality test failed. We assessed statistical significance, as appropriate, by performing one-way ANOVA, the Mann-Whitney rank sum test or the Kolmogoroff-Smirnoff test. We performed statistical analysis with Sigma Stat 3.5 and Origin 7.0 (Microcal Software). Statistical box charts show the mean (central dot), median (large horizontal line), 99% and 1% range (crosses), 25–75% percentile range (box), and 5–95% percentile range (whiskers) (see Fig. 3a). The

experiments reported here were not performed by blinded observers, as relevant analyses, such as seizure detection were performed by standardized and/or automated routines.

Optogenetics—*Stereotactic viral injections* were carried out as previously described[15]. Briefly, we kept the rats under isoflurane anesthesia in a stereotactic frame. We performed craniotomies so as to cause minimal damage to cortical tissue. We injected virus carrying genes for fluorescent proteins and eNpHR (rAAV5/CamKIIα-eNpHR-EYFP), or for fluorescent proteins alone (rAAV5/CamKIIα-EYFP), stereotaxically *in vivo* into the right somatosensory VB thalamus 1–2 weeks after stroke induction or Rose Bengal treatment in injured and control rats, respectively. Injection of viral DNA under CamKIIα promoter results in expression only in excitatory thalamic neurons[15]. 500 nl of the concentrated virus suspension (2×10^{12} genome copies per milliliter) was infused into VB thalamus using a 10-μl syringe and 34-gauge needle. We controlled the injection rate (100 nl/min) by pump (World Precision Instruments). The stereotaxic coordinates of the injections were 2.6–2.7 mm posterior to Bregma, 2.8 mm lateral to the midline and 5.8–6.0 mm below the cortical surface.

For in vitro optogenetics and slice electrophysiology we sacrificed the subjects 2–3 months after viral injections corresponding to P100–140 and we made acute horizontal brain thalamic slices for optical stimulations and *in vitro* recordings. We prepared thalamic slices and performed *in vitro* whole-cell recordings as described above. We visualized eNpHR-expressing VB neurons with fluorescence microscopy. We stimulated eNpHR-expressing neurons with yellow laser stimuli (594 nm, 0.7 mW to 20 mW, 200 ms – 5 s flashes; OEM Laser Systems) delivered with optic fiber (BFL 37–300, Thor Labs) (see schematic diagrams in Supplemental Fig. 1b right). At the end of the recordings, we fixed the slices with 4% paraformaldehyde (wt/vol) solution, then resectioned at 80 μm and low- and high-magnification images were obtained with fluorescence (Nikon) and confocal (Zeiss LSM 510) microscopes, respectively. We obtained both coronal cortical and horizontal thalamic slices from the same rats to confirm the presence and location of eNpHR-expressing VB TC axons and terminals in the somatosensory cortex (Fig. 5b). TC neurons were recorded from VB thalamus. eNpHR3.0 expression was restricted to glutamatergic TC neurons in VB and was not observed in RT GABAergic neurons (Supplemental Fig. 9). Virus spread was reproducible across subjects. eNpHR current was similar in VB cells from control and injured rats and the stimulation intensity and duration required to silence eNpHR-expressing TC cell firing was reproducible and similar in control and injured subjects, suggesting that virus expression in TC cells was comparable in control and injured subjects.

Chronic optrode recordings in freely behaving subjects. 2–3 weeks after viral injections in VB, we anesthetized the subjects[15] and implanted a chronic device containing 5 EEG screws, 1 EMG wire to record electromyographic activity, and an optrode targeting the VB thalamus in control and injured rats. Optrodes[26] containing 4 tungsten depth electrodes and a 200um-core, NA=0.37, optical fiber (Supplemental Fig. 7d) were stereotactically inserted to a depth of 5.3 mm as depicted in Fig. 5a). We delivered yellow laser light (594 nm) into the thalamus *via* an optical fiber to inhibit eNpHR3.0–expressing thalamocortical neurons. Arrays were designed to sample from a large thalamic volume. EEG screws (2.38-mm-long #303SS, J.J. Morris) were attached to stainless steel wires (Medwire 316 SS 7/44T). We

stabilized the devices on the skull with dental cement (C&B MetaBond). We conducted experiments in freely behaving animals between 2 weeks and 10 months after device implantation. For recordings, we placed the subjects in a dedicated glass-walled chamber that allowed for video monitoring. We attached a custom-made buffering headstage amplifier to the animal to allow for recording from high-impedance depth LFP electrodes, and attached to a XLTek 32 Channel EEG headbox via a 50-cm, 12 channel cable with inline electrical commutator (Plastics One). We sampled EEG recordings at 500 Hz. In the manuscript, we refer to electrocorticographic signals recorded with skull screws as “EEG” recordings.

To define whether the rat was epileptic or not we used the classification proposed by the International League Against Epilepsy and the International Bureau for Epilepsy, that is, epilepsy can be considered if there is an enduring alteration in the brain –here the cortical lesion - and at least two seizures.

Optical Stimulation in freely-behaving subjects: For optical stimulation experiments, a 594 nm DPSS laser (OEM Laser Systems) was operated continuously at high output power for optimal stability. Output light power was reduced by neutral density filters, and stimulation was gated by a silent, low-latency beam shutter (SRS-475, Stanford Research Systems). The output beam was coupled into a 200um-core, NA=0.37 fiber optic cable, with an inline fiber optic rotating joint (Doric Lenses). This fiber was passed through a concentric channel in the electrical commutator before attaching to the animal to allow for free rotation of the animal during extended experiments. Light power levels are reported for the end of the cable before attachment to the implant.

Real-time seizure detection and disruption in freely behaving animals: For real-time seizure disruption experiments, we routed a single cortical EEG channel showing clear seizure activity from the recording system to a programmable real-time digital signal processor (RP2.1, Tucker-Davis Technologies). The processor digitized the signal at 6kHz, applied a bandpass filter (1–40Hz), then calculated the line-length[29] in a sliding window of 2 seconds, updated at 6kHz. Line-length threshold for seizure detection was set manually for each animal at the beginning of the experiment. Upon upward crossing of the threshold, the system randomly triggered either laser stimulation for either 0.5 or 10 s (by opening the beam shutter) or sham stimulation. An 11-second timeout was imposed after each detection event to prevent retriggering and allow for analysis of response to the stimulation.

We analyzed data in Matlab, using custom software. We performed spectral analysis using the wavelet method with Matlab (MathWorks)[22].

EEG power quantification in freely behaving subjects: A basis of Morlet wavelets from 1–128 Hz was used, with 10 wavelets per octave. Power at a given frequency was obtained using the inner product of a Morlet wavelet with the raw signal, and then squared. To account for logarithmic frequency sampling, power was divided by the period for bias correction[30]. To remove the 1/f bias inherent in biological signals, the power was normalized by the mean power at each frequency, resulting in spectrograms with unitless power (Figs. 5d and 7c,d; Supplemental Figs. 7a and 8a). In some cases, the power spectrum

was smoothed using a boxcar filter of length 0.25 s. Spectrograms were aligned based on a signal corresponding to the opening of the laser shutter, different trials were averaged together, and were plotted over time. For computation of signal power across the spectrum, the raw signal was bandpass filtered from 1–50 Hz, and the root-mean-square (RMS) amplitude was obtained. The effect of the laser trigger on the EEG and LFP signals was quantified by comparing the RMS averaged two seconds before and after the trigger (Fig. 5e,f; Supplemental Figs. 7c and 9a,b).

Multi-unit firing quantification in freely behaving subjects: We recorded multi-unit thalamic depth recordings using a multiplexing headstage amplifier (M32, Triangle Biosystems) connected to a multichannel neural recording system (Digital Cheetah, Neuralynx). Signals were bandpass filtered from 600–6000 Hz to detect spiking activity. Deflections below negative 40μV were marked as putative spike events. We computed the duration and amplitude by which the signal exceeded threshold, and we exluded events with parameters more than 2 standard deviations (SD) from the mean. For calculation of rates, events were counted in 1–2 sec bins, divided by the bin size. We discarded trials in which there was a transient of greater than 500 μV or the count was 3 SD away from the median. Bins with the same temporal offset were used to calculate average spike rates across trials.

Immunohistochemistry: We performed histology as described in[19]. Briefly, animals that had undergone behavioral analysis were anesthetized with pentobarbital (200 mg/kg, i.p.) and perfused transcardially with saline followed by 4% paraformaldehyde (Sigma-Aldrich) in 0.1 M phosphate buffer (Sigma-Aldrich), pH 7.4. We removed the brains and postfixed in 4% phosphate-buffered paraformaldehyde at 4°C overnight. We took digital images for documentation of the position and extent of lesions (see Supplemental Fig. 6), and we cryoprotected the brains with 30% sucrose. We obtained horizontal or coronal 50 μm sections with a sliding freezing microtome (Microm; HM 400). We processed sections for immunofluorescence for glial fibrillary acidic protein 1:1000(GFAP) (Millipore Temecula CA) and in some cases for HCN2 1:500 and HCN4 1:500 (kindly provided by Prof. Ryuichi Shigemoto, Okazaki, Japan). We incubated the sections for one hour in Normal Donkey Serum and then in primary antibodies diluted in PBS plus Triton X for 48 hours, rinsed in PBS and incubated with a secondary fluorescent antibody (Jackson Immuno Research) at a concentration of 1 μg/ml. We mounted the sections on slides using Vectashield Mounting Media (Vector Labs Burlingame CA) and assessed the immunofluorescence with a laser confocal microscope (Zeiss LSM 510).

Morphological identification and HCN2 and HCN4 protein quantification: We filled the cells with 0.2–0.5% biocytin (Sigma-Aldrich) included in the internal solution of the recording electrode. We fixed whole slices and processed them using the standard avidin–biotin peroxidase method (Horikawa and Armstrong, 1988; Tseng et al., 1991). We processed slices for immunofluorescence for glial fibrillary acidic protein (GFAP) (Millipore), HCN2 and HCN4 (kindly provided by Prof. Ryuichi Shigemoto, Okazaki, Japan). We assessed immunofluorescence with a laser confocal microscope (Zeiss LSM 510). We assessed HCN2 and HCN4 protein expression for each biocytin-filled cell by measuring the volume of HCN2 and HCN4 particles. We obtained confocal z-stack images

with an optical distance of 0.5 μm from the soma and dendritic processes of biocytin labeled cells. Each z-stack image was rendered into a 3D image (Volocity 2.6.1; Improvision Ltd.) where signals from each fluorophore were analyzed separately. Voxels occupied by biocytin labeled cells, HCN 2 and HCN4 immunoreactivity were detected with consistent fluorescence signal threshold intensities throughout the analysis.

Computational modeling: We built a minimal computational model of the negative feedback loop between TC cells and RT neurons to assess the oscillatory response of thalamic slices. We used a Hodgkin-Huxley style biophysical model to describe TC cell excitability, with parameters fitted from whole-cell recordings in control and injured conditions.

In the TC cell model we consider, the potential follows $C_m \dot{V} = -(I_L + I_{Na} + I_K + I_T + I_H) + I_{inj} + I_{GABA}$, where the leak current is $I_L = \overline{g_L}(V - V_L)$, I_{Na} and I_K are taken from Wang (1994) and I_T from Huguenard and McCormick (1992), and $I_H = \overline{g_H} m_H (V - V_H)$, with activation following $\tau_H(V)\dot{m}_H = m_H^\infty(V) - m_H$ with $\tau_H(V) = \tau_{min} + (\tau_{max} - \tau_{min})/(e^{-(V-V_{H1/2})/k_H} + e^{(V-V_{H1/2})/k_H})^{-1}$ and $m_H^\infty(V) = \left(1 + \exp\left(-(V - V_{H1/2})/k_H\right)\right)^{-1}$, with parameters fitted from whole-cell patch clamp recordings. Parameters were $C_m = 1\mu F cm^{-2}$, $\overline{g_L} = 0.025 mS cm^{-2}$, $V_L = -75mV$, $\overline{g_{Na}} = 35 mS cm^{-2}$, $V_{Na} = 55mV$, $s_{Na} = 5mV$, $\overline{g_K} = 25 mS cm^{-2}$, $V_K = -80mV$, $s_K = 18mV$, $\overline{g_T} = 0.025 mS cm^{-2}$, $V_T = 120mV$, $\overline{g_H} = 0.5 mS cm^{-2}$, $V_H = -40mV$, $V_{H1/2} = -105mV$, $k_H = 10$, $\tau_{min} = 1000ms$ and $\tau_{max} = 6000ms$. In injured TC neurons, we set $V_{H1/2} = -95mV$, $\tau_{min} = 500ms$ and $\tau_{max} = 3500ms$ to fit the $+10mV$ shift of the steady-state activation curve and the decreased voltage-dependent time constant. Injured neurons have a membrane surface area $S = \alpha S_0$, where S_0 is the area of control neurons ($\alpha = 0.5$). This modification accounted for the increased input resistance $(R_{in} \approx g_L^{-1} S^{-1} = g_L^{-1} \alpha^{-1} S_0^{-1} = \alpha^{-1} R_{in0})$ and unchanged time constant $(\tau = C_m S g_L^{-1} S^{-1} = C_m g_L^{-1} = \tau_0)$. To model the absence of any additional noticeable modification of intrinsic conductance, the maximal conductance of voltage-dependent conductance was considered constant $(\overline{g_X} S = \overline{g_{X0}} S_0)$, i.e. the number of channels is regulated by some homeostatic mechanism opposing the effects of the neocortical infarction (e.g. intrinsic plasticity; see [31]). To model the negative feedback loop characterizing the thalamic network, we considered that every TCR spike excited a small population of RE neurons, resulting in a $GABA_A$-mediated population IPSP of 25 spikes (5 individual IPSPs from 5 RE neurons) with uniformly distributed random delays in the range $[0;2\delta t]ms$ due to synaptic transmission and integration in RE neurons. The GABA current was $I_{GABA} = \overline{g_{GABA}} x_{GABA}(V - V_{GABA})$ with $\dot{x}_{GABA} = -x_{GABA}/\tau_{GABA} + (1 - x_{GABA}) \sum_k \delta(t - t_k)$, where $\delta()$ is the Dirac function and t_k represent RE spike arrival times. An population IPSP was applied at t_0 to trigger an initial rebound burst and initiate the network oscillatory response (duration $d = t_{Last\ TCR\ Spike} - t_0$), which was classified as silent (no TCR spike), transient ($d \leq t_{Simulation}$) or infinite ($d > t_{Simulation}$). Response maps were built as a function of the injected current mimicking constant cortical input (I_{inj}) and the strength of the intra-

thalamic feedback ($\overline{g_{GABA}}$). Oscillation duration differences were computed in the domain of transient oscillations, the behavior observed in TC neurons and expressed as a function of the resting membrane potential ($V_R(I_{inj})$, instead of I_{inj}) of control neurons, to examine whether they indeed occurred in the physiological range encountered in whole-cell patch clamp recordings, i.e. $[-75;-65]mV$. $\overline{g_{GABA}}$ was as described in respective figures and we used $\delta t = 25ms$, $\tau_{GABA} = 20ms$, $V_{GABA} = -85mV$ and $t_{Simulation} = 2s$. Therapeutic conditions were set as following:

$$\begin{aligned}\overline{g_L} &= 0.075 mS cm^{-2} (\mathrm{T/gL\ \ condition}), \overline{g_h} \\ &= 0.1 mS cm^{-2} (\mathrm{T/gL\ \ condition}), \overline{g_L} \\ &= 0.075 mS cm^{-2} \text{ and } \overline{g_h} \\ &= 0.2 mS cm^{-2} (\mathrm{T/gL{+}gH\ \ condition}).\end{aligned}$$

Supplementary Material

Refer to Web version on PubMed Central for supplementary material.

Acknowledgements

J.T.P. is supported by NIH-NINDS K99NS078118-01 and Epilepsy Foundation. J.R.H. is supported by NIH-NINDS 5R01NS006477 and 5R01NS034774. T.J.D. is supported by Berry Foundation Postdoctoral fellowship. K.D. is supported by Howard Hughes Medical Institute, CIRM, NIH and DARPA REPAIR Program. E.S.F. is supported by Epilepsy Foundation Postdoctoral Fellowship. We thank Carl Pisaturo for designing and fabricating custom electronics, Anne Herbert and Sha Jin for their help with animal husbandry and Kevin Graber and David Prince for discussions related to clinical aspects of post-stroke epilepsy.

REFERENCES

1. Clarkson AN, Huang BS, Macisaac SE, Mody I, Carmichael ST. Reducing excessive GABA-mediated tonic inhibition promotes functional recovery after stroke. Nature. 2010; 468:305–309. [PubMed: 21048709]
2. Kotila M, Waltimo O. Epilepsy After Stroke. Epilepsia. 1992; 33:495–498. [PubMed: 1592026]
3. Kelly KM. Animal modeling of poststroke seizures and epilepsy: 5-year update. Epilepsy Curr. 2007; 7:159–162. [PubMed: 18049725]
4. Lee J-C, et al. Seizures in childhood ischemic stroke in Taiwan. Brain Dev. 2009; 31:294–299. [PubMed: 18650041]
5. Kwan P, Brodie MJ. Early identification of refractory epilepsy. N. Engl. J. Med. 2000; 342:314–319. [PubMed: 10660394]
6. Loiseau P Pathologic processes in the elderly and their association with seizures. Seizures and Epilepsy in the Elderly. 1997:63–85.
7. Hoffman SN, Salin PA, Prince DA. Chronic neocortical epileptogenesis in vitro. J. Neurophysiol. 1994; 71:1762–1773. [PubMed: 8064347]
8. Huguenard JR, Prince DA. Basic mechanisms of epileptic discharges in the thalamus. The Thalamus. 1997; 2:295–330.
9. Bruehl C, Kloiber O, Hossman KA, Dorn T, Witte OW. Regional hypometabolism in an acute model of focal epileptic activity in the rat. Eur. J. Neurosci. 1995; 7:192–197. [PubMed: 7757256]
10. Detre JA, Alsop DC, Aguirre GK, Sperling MR. Coupling of cortical and thalamic ictal activity in human partial epilepsy: demonstration by functional magnetic resonance imaging. Epilepsia. 1996; 37:657–661. [PubMed: 8681898]
11. Redecker C, Bruehl C, Hagemann G, Binus O, Witte OW. Coupling of cortical and thalamic metabolism in experimentally induced visual and somatosensory focal epilepsy. Epilepsy Res. 1997; 27:127–137. [PubMed: 9192187]

12. Gasteiger EL, Albowitz B, Barken FM. Interictal afterdischarge in focal penicillin epilepsy: block by thalamic cooling. Exp. Neurol. 1985; 88:349–359. [PubMed: 3921396]
13. Mondragon S, Lamarche M. Suppression of motor seizures after specific thalamotomy in chronic epileptic monkeys. Epilepsy Res. 1990; 5:137–145. [PubMed: 2328715]
14. Tye KM, Deisseroth K. Optogenetic investigation of neural circuits underlying brain disease in animal models. Nature Reviews Neuroscience. 2012; 13:251–266. [PubMed: 22430017]
15. Paz JT, et al. A new mode of corticothalamic transmission revealed in the Gria4(−/−) model of absence epilepsy. Nat. Neurosci. 2011; 14:1167–1173. [PubMed: 21857658]
16. Tønnesen J, Sørensen AT, Deisseroth K, Lundberg C, Kokaia M. Optogenetic control of epileptiform activity. Proc. Natl. Acad. Sci. U.S.A. 2009; 106:12162–12167. [PubMed: 19581573]
17. Kelly KM, et al. Photothrombotic brain infarction results in seizure activity in aging Fischer 344 and Sprague Dawley rats. Epilepsy Res. 2001; 47:189–203. [PubMed: 11738927]
18. Kharlamov EA, Jukkola PI, Schmitt KL, Kelly KM. Electrobehavioral characteristics of epileptic rats following photothrombotic brain infarction. Epilepsy Res. 2003; 56:185–203. [PubMed: 14643003]
19. Paz JT, Christian CA, Parada I, Prince DA, Huguenard JR. Focal cortical infarcts alter intrinsic excitability and synaptic excitation in the reticular thalamic nucleus. J. Neurosci. 2010; 30:5465–5479. [PubMed: 20392967]
20. Reid CA, Phillips AM, Petrou S. HCN channelopathies: pathophysiology in genetic epilepsy and therapeutic implications. Br. J. Pharmacol. 2012; 165:49–56. [PubMed: 21615728]
21. Huguenard JR, Prince DA. Intrathalamic rhythmicity studied in vitro: nominal T-current modulation causes robust antioscillatory effects. J. Neurosci. 1994; 14:5485–5502. [PubMed: 8083749]
22. Schofield CM, Kleiman-Weiner M, Rudolph U, Huguenard JR. A gain in GABAA receptor synaptic strength in thalamus reduces oscillatory activity and absence seizures. Proc. Natl. Acad. Sci. U.S.A. 2009; 106:7630–7635. [PubMed: 19380748]
23. Bryant AS, Li B, Beenhakker MP, Huguenard JR. Maintenance of thalamic epileptiform activity depends on the astrocytic glutamate-glutamine cycle. J. Neurophysiol. 2009; 102:2880–2888. [PubMed: 19741104]
24. Karhunen H, et al. Epileptogenesis after cortical photothrombotic brain lesion in rats. Neuroscience. 2007; 148:314–324. [PubMed: 17629408]
25. Gradinaru V, et al. Molecular and cellular approaches for diversifying and extending optogenetics. Cell. 2010; 141:154–165. [PubMed: 20303157]
26. Yizhar O, et al. Neocortical excitation/inhibition balance in information processing and social dysfunction. Nature. 2011; 477:171–178. [PubMed: 21796121]
27. Esteller R, Echauz J, Tcheng T, Litt B, Pless B. Line length: an efficient feature for seizure onset detection. Engineering in Medicine and Biology Society, 2001. Proceedings of the 23rd Annual International Conference of the IEEE. 2001; 2:1707–1710. vol.2.
28. McCormick DA, Pape HC. Properties of a hyperpolarization-activated cation current and its role in rhythmic oscillation in thalamic relay neurones. J. Physiol. (Lond.). 1990; 431:291–318. [PubMed: 1712843]
29. Esteller R, Echauz J, Tcheng T, Litt B, Pless B. Line length: an efficient feature for seizure onset detection. Engineering in Medicine and Biology Society, 2001. Proceedings of the 23rd Annual International Conference of the IEEE. 2001; 2:1707–1710. vol.2.
30. Torrence C, Compo G. A Practical Guide to Wavelet Analysis. Bulletin of the American Meteorological Society. 1997; 79:61–78.
31. Marder E, Goaillard J-M. Variability, compensation and homeostasis in neuron and network function. Nature Reviews Neuroscience. 2006; 7:563–574. [PubMed: 16791145]
32. Zhang Q, Huang A, Lin Y-C, Yu H-G. Associated Changes in HCN2 and HCN4 Transcripts and If Pacemaker Current in Myocytes. Biochim Biophys Acta. 2009; 1788:1138–1147. [PubMed: 19236845]

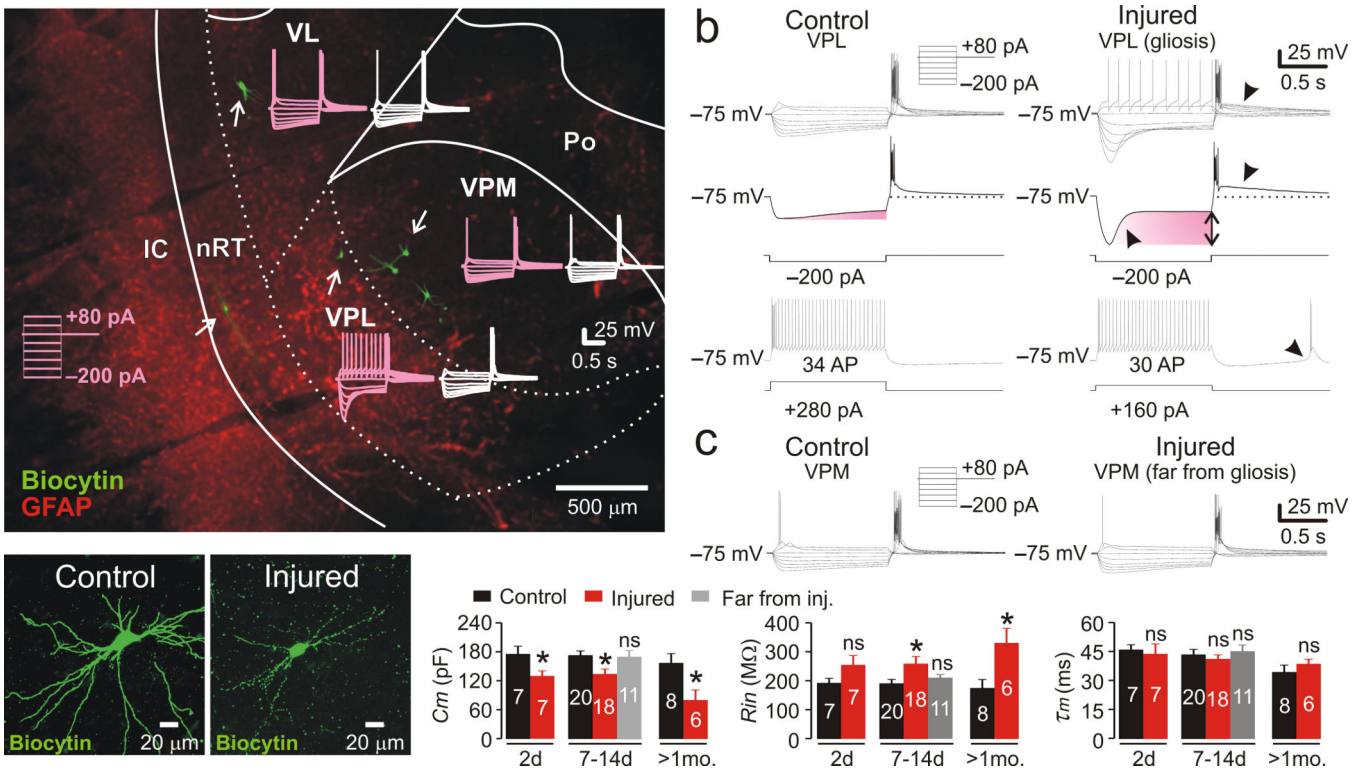

Figure 1. Cortical stroke results in enhanced intrinsic excitability in TC neurons

a, Confocal image of a horizontal thalamic slice ipsilateral to the stroke (7 days post-stroke) with GFAP immunolabeling and thalamic neurons labeled by intracellular injection of biocytin (green, see arrows) during recordings. Pink traces: responses to intra-cellular injection of current pulses (from −200 pA to +80 pA) in TC cells from different thalamic nuclei ipsilateral to the infarct. White traces: responses from TC cells in control rats using the same protocols from corresponding nuclei. **b–c,** Representative voltage responses to current injections in TC cells from an injured and a control rat. Note the enhanced intrinsic rebound properties in injured cells (arrowheads: larger post-inhibitory after-depolarization, enhanced hyperpolarization-activated sag and post-hyperpolarization burst). **d,** Confocal images of representative control and injured TC neurons (7 days post-stroke). **e,** Passive membrane properties: capacitance (Cm), input resistsance (Rin) and membrane time constant (τm) in TC cells within or far (>200µm) from gliosis at 2 days, 7–14 days and >1 month post-stroke (mean ± s.e.m.; *p<0.05; ns, p>0.1; one-way ANOVA). Number of cells is indicated for each group. Data are from 9 control and 12 injured rats. AP, action potential; IC, internal capsule; nRT, Po, VL, VPL, VPM: reticular, posterior, ventrolateral, ventroposterolateral and ventroposteromedial thalamic nuclei.

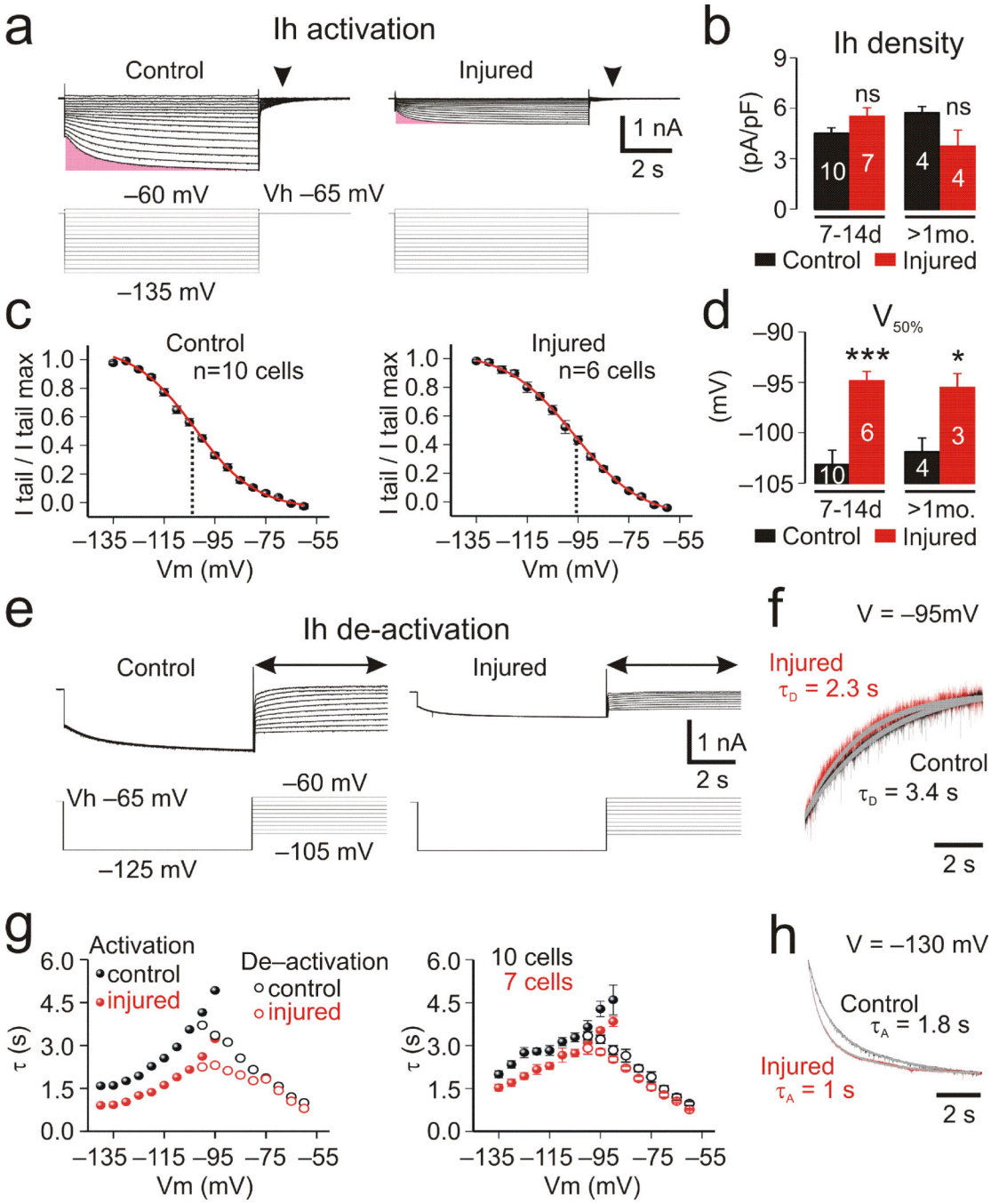

Figure 2. Cortical stroke alters biophysical properties of Ih in TC neurons

a–d, Ih activation. **a,** Current responses (top traces) to voltage steps (bottom traces) in representative TC cells from an injured and a control rat. Ih was measured at the tail current (arrowheads) (see Methods for details). **b,** The density of Ih at maximal activation was similar (ns, p>0.1) in TC cells from injured and control rats at both 7–14d and at >1mo. Post-stroke. **c,** Ih voltage-dependent activation curves 7–14d post-stroke: average plot of normalized Ih amplitude as a function of membrane potential, best fitted with a Boltzmann function (R^2=0.99, both fits). **d,** Half-activation voltage ($V_{50\%}$) of Ih was shifted towards

depolarized values after injury (*p<0.05; ***p=0.001). **e,** Ih de-activation protocol. Voltage-dependence of Ih de-activation was examined by fully activating Ih at −125mV and then stepping to membrane potentials between −105 and −60mV. De-activation time constant (τ_D) was calculated from exponential fits performed on the traces indicated by double-ended arrows. **f,** expanded de-activation currents traces obtained at −95mV voltage step from the cells depicted in **e**. **g,** Time constants of Ih activation and de-activation from the two representative cells (**g, left**) and averaged across all the cells (**g, right**). **h,** Ih activation currents during −130mV voltage step (from cells in **a**) were best fitted with a single-exponential function (grey lines). **b,c,d,g:** Data are from 5 control and 3 injured rats. **a,e,f,g** are from the same representative control and injured cells. The number of cells is indicated in the panels. Quantitative data: mean ± s.e.m. Statistical significance: one-way ANOVA.

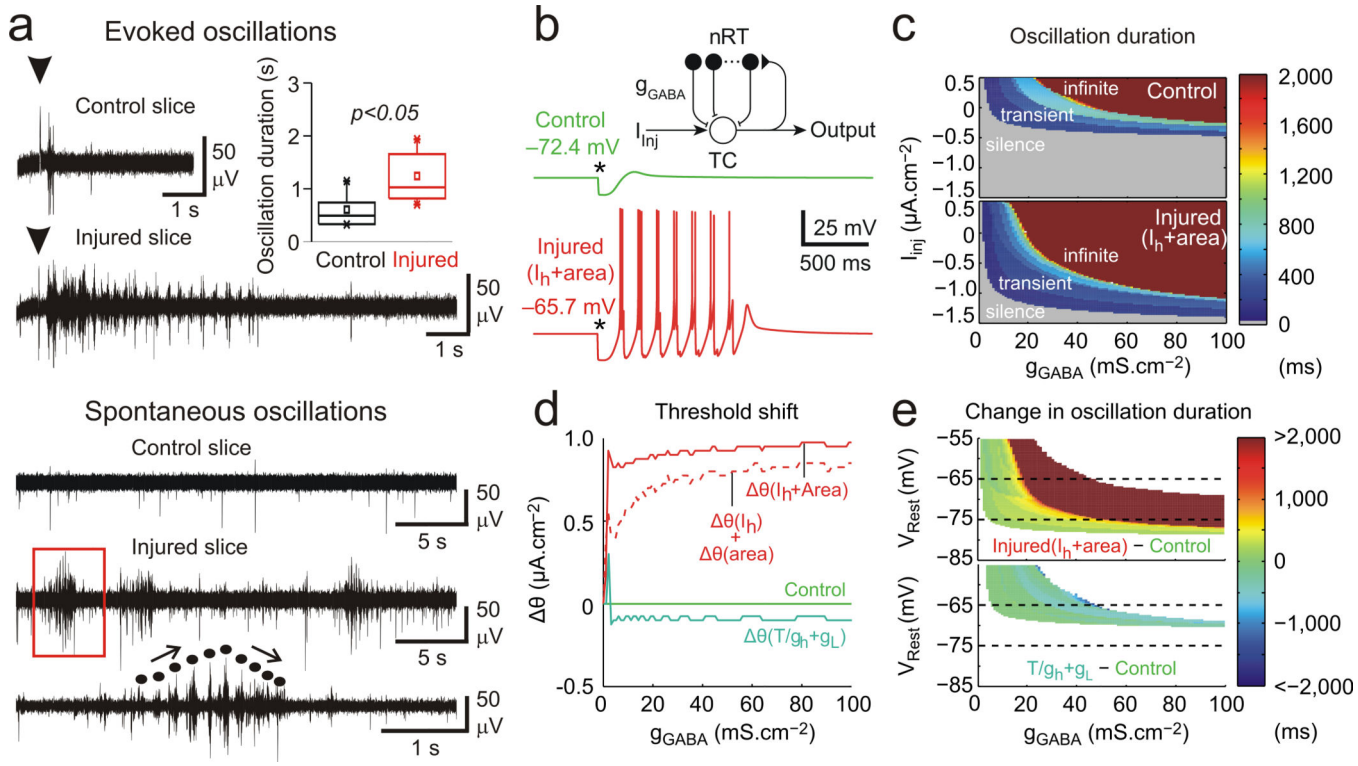

Figure 3. Intra-thalamic network is hyperexcitable and generates epileptiform oscillations in injured animals and in a model

a top: Multiunit recordings in thalamic slices ipsilateral to cortical stroke depicting network oscillations evoked by single electrical shocks (arrowheads) to internal capsule. Inset: box charts of oscillation duration from 3 control rats (n=5 slices) and 3 injured rats (n=8 slices); one-way ANOVA. **a bottom:** Representative spontaneous activities. Red box: recording enlarged on the bottom trace. Note the crescendo, decrescendo pattern of the oscillation (dots and arrows). **b–e,** Results from computational modeling. **b,** (top) Minimal thalamus model including a TC neuron, negative feedback through RT neurons (g_{GABA}) and a constant steady state cortical input current (I_{inj}). (bottom) Changes in intrinsic excitability ("Ih+area": altered activation of both Ih and membrane area) promote epileptiform TC response in the network. **c,** The map of oscillation duration as a function of the RT-TC feedback (g_{GABA}) and the injected input current (I_{inj}) indicates that, in injured conditions, a larger hyperpolarizing current (I_{inj}) is required to prevent the initiation of oscillations. In the text "threshold for oscillation initiation" refers to the threshold value of I_{inj} above which an oscillation is initiated. **d,** Difference in threshold for oscillation initiation between control and different injured conditions: Δθ (Ih+area) (solid red) when combining altered area and altered Ih activation; or Δθ(Ih)+Δθ(area) (dashed line) when adding separate effects of altered area and altered Ih activation; or following combined therapeutic conditions with modified h and leak conductances (Δθ(T/g_h+g_L), bluish green). "Threshold" (θ) is input current (I_{inj}) threshold for initiation of oscillations. **e,** Difference in oscillation duration between control and injured conditions as a function of g_{GABA} within the physiological range of resting membrane potential (dashed lines). Duration is increased in injured conditions (top) and restored to control level under therapeutic conditions (bottom). "Ih":

only Ih activation is altered (Fig. 2); “area”: only membrane area is altered (lower Cm: Fig. 1 and Methods). “Ih+area”: both properties are altered. See text and Supplemental Figs. 4 and 5 for details.

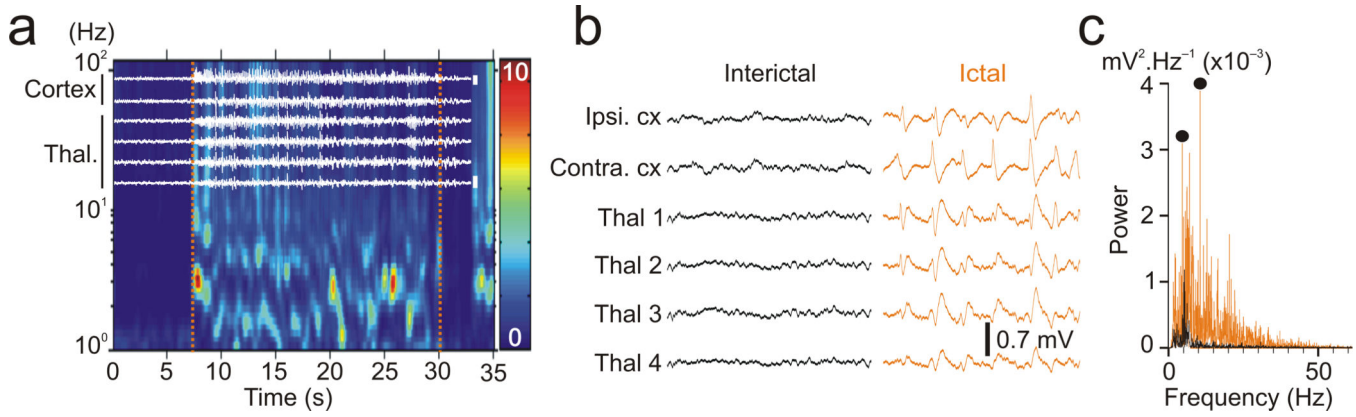

Figure 4. Cortical stroke leads to late spontaneous epileptic activities in cortex and thalamus

a, EEG wavelet spectrogram from a representative cortical channel (top trace). Vertical dashed lines indicate the onset and the end of the electrographic seizure activity. White traces represent simultaneous cortical EEG and thalamic LFP recordings, temporally aligned with the wavelet spectrogram. **b,** Representative 1-s-long ictal and interictal EEG recordings from the recordings depicted in **a**. **c,** Corresponding power spectra of ictal (orange) and interictal (black) EEG activities from ipsi. cx channel. Dots indicate the dominant peak frequencies during ictal periods (4–5 and 8–10 Hz). The depicted recordings were obtained 6.5 months after stroke induction from a 7.5-month old rat.

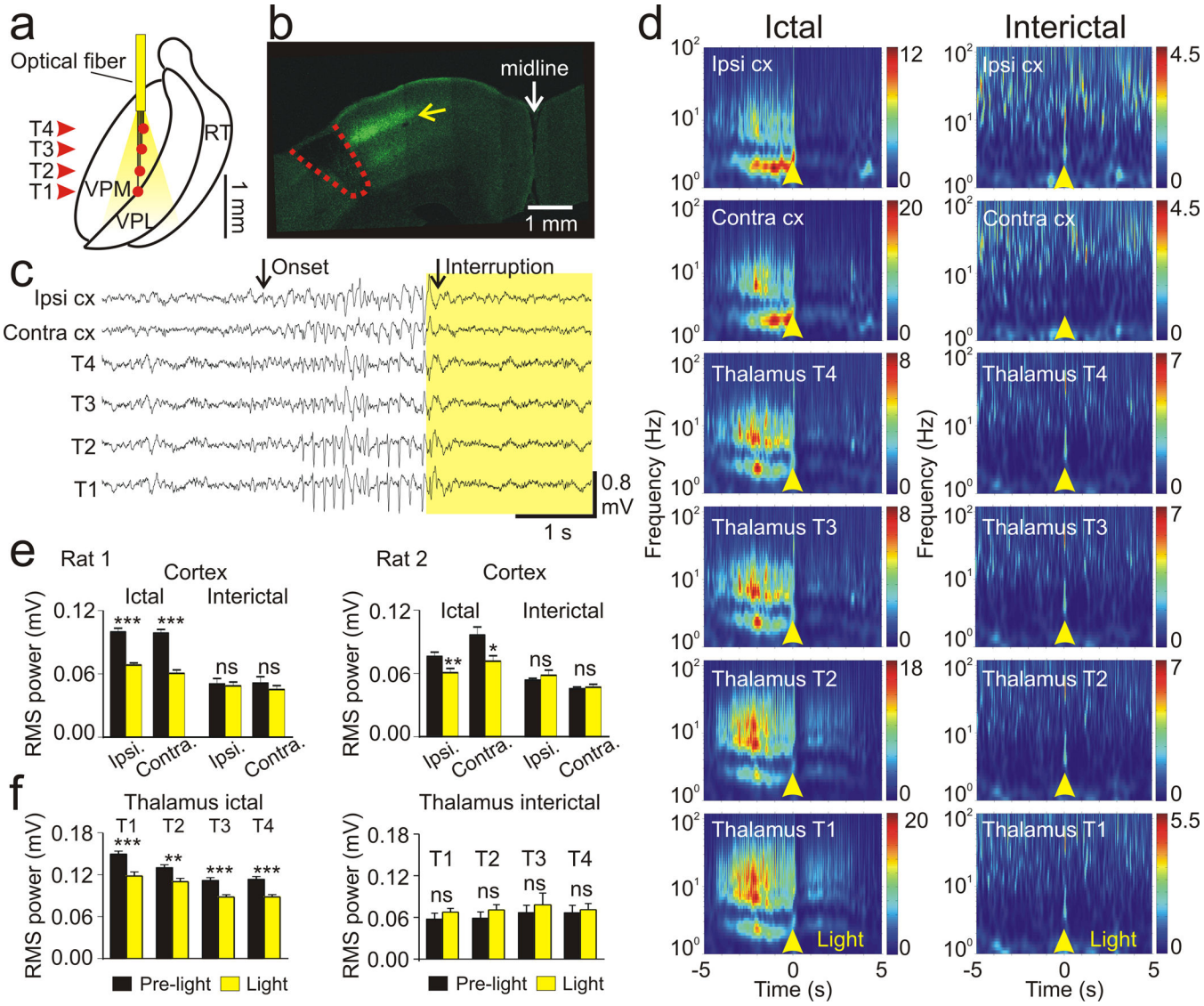

Figure 5. Selective optical inhibition of TC neurons interrupts ongoing epileptic seizures in awake, freely behaving animals

a, Diagram of chronic multisite optrode (CMO) implanted into somatosensory thalamus for behaving recordings/optical stimulations. Arrowheads indicate thalamic recording sites (T1–4). **b,** Confocal image of coronal brain section taken through the cortical lesion (red dashed line) showing Camk2α:eNPHR-expressing TC fibers terminating mainly in layer 4 (yellow arrow) from a rat sacrificed after recordings. **c,** Representative example of simultaneously recorded cortical EEGs and thalamic LFPs before and during 594 nm light delivery in the thalamus ipsilateral to stroke. Arrows indicate seizure onset and its interruption by light delivery in thalamus. **d,** Mean spectrograms of thalamic LFPs and cortical EEGs from the same rat. 594 nm light pulses were delivered in VPM at time 0. Shown are examples from all stimulations (ictal: n=19; interictal: n=4) from a single recording session ~4.2 months post-stroke, 4 months post-viral delivery in thalamus. **e–f,** power quantification of cortical EEGs **(e)** and thalamic LFPs **(f)** before and during light delivery in thalamus (**e left**: ictal:

n=56 events from 3 different trials; interictal: n=8 events from 2 different trials; **e right**: ictal: n=6 events from 2 different trials; interictal: n=11 events from 2 different trials). **e left** and **e right** are from 2 different rats. **e left** and **f** are from the same rat. RMS (root-mean-square) power was averaged 2s before and 2s during light delivery (see Methods for details). Error bars: s.e.m.. ns, $p \geq 0.1$ (not significant); *$p<0.05$; **$p<0.01$; ***$p<0.0001$; Paired t-test or Signed Rank test, as appropriate. Results in **c–f** were obtained using light at 10 mW.

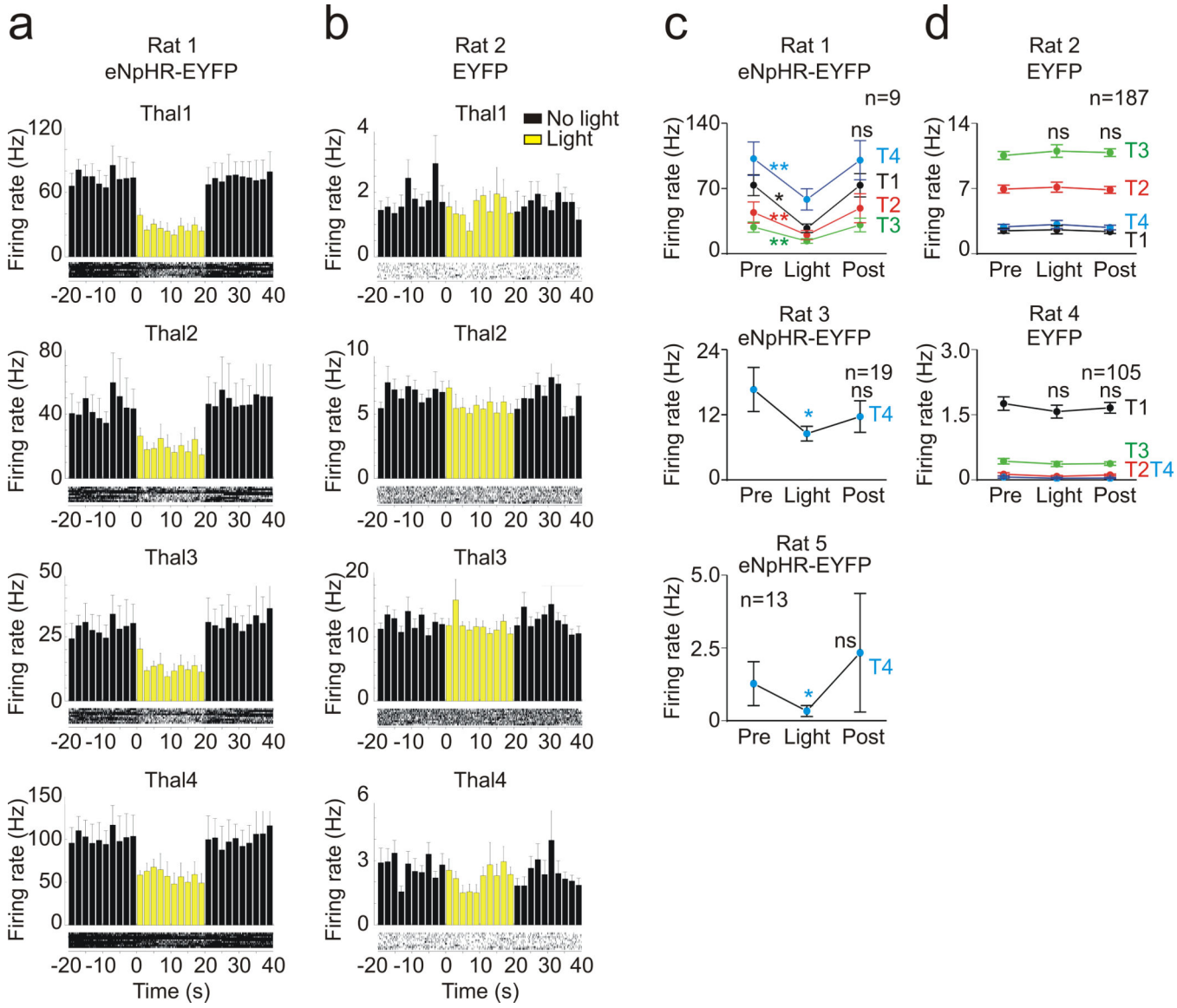

Figure 6. Multiunit firing of TC neurons in awake, freely behaving animals

a,b, Histograms representing the mean multiunit firing frequency of TC neurons (bin, 2 s) at the indicated times before, during and after a 20s light pulse delivery in the thalamus (594 nm, 10 mW; n=9 repetitions within a trial). **a–b**, Multiunit firing was recorded simultaneously at 4 thalamic locations (T1–4, see CMO diagram in Supplemental Fig. 7d). Corresponding raster plots are presented at the bottom of each histogram. Data in **(a)** and **(b)** are from two different rats: **(a)**: a rat with eNpHR:EYFP+ TC neurons; **(b)**: a rat with EYFP + TC neurons, not expressing eNpHR. **(a)** is from a rat with no stroke; **(b)** is from a rat with stroke. **c–d,** Multiunit firing rate averaged 20 s before, 20 s during and 20 s after light illumination of the thalamus. The number of sweeps is indicated in each graph. **a** and **c** *top* are from the same rat. **b** and **d** *top* are from the same rat. Each graph in **c** and **d** is from a different rat illustrating reproducibility of light effects between rats. “Rat5” corresponds to the same rat as in Fig. 5c,d,e left, f in which thalamic illumination disrupted seizures. Data

correspond to mean ± s.e.m. ns, $p>0.1$. *$p<0.05$; **$p<0.01$. Statistical significance: paired t-test or signed rank test, as appropriate. Only data from channels from which we were able to quantify firing are presented. Firing was not detected in all the thalamic channels.

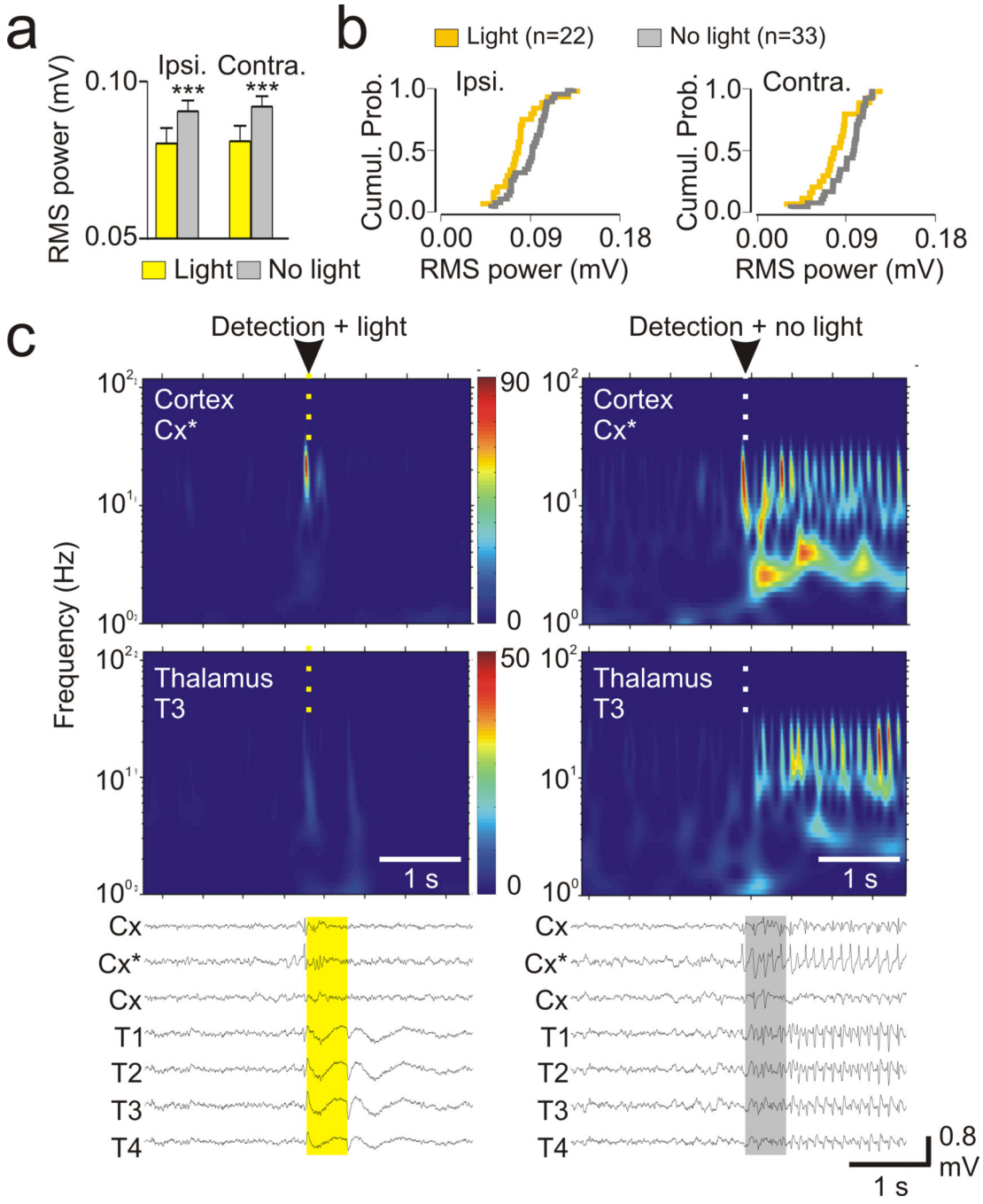

Figure 7. Online detection and interruption of seizures *via* a 594 nm light illumination of thalamus in freely behaving animals

a, Upon an automatic detection of seizure activity the system randomly triggered either yellow light (yellow) or sham stimulation (grey, no light). **a,** RMS power of ipsi- and contra-lateral EEGs in 2 s period following seizure detection in presence of yellow light in the thalamus (n=22 events) or during sham stimulation (n=33 events). **b,** Corresponding cumulative probability distribution of the average RMS power with or without the light. **c,** Top: Representative spectrograms from a cortical EEG and a thalamic LFP in the yellow

light (left) or sham (right) conditions. Bottom: corresponding recordings of cortical EEGs (Cx) and thalamic LFPs (T1–4). The spectrograms and the electrophysiological recordings are temporally (vertically) aligned. Data in c were obtained using 0.5 s - long light pulses.

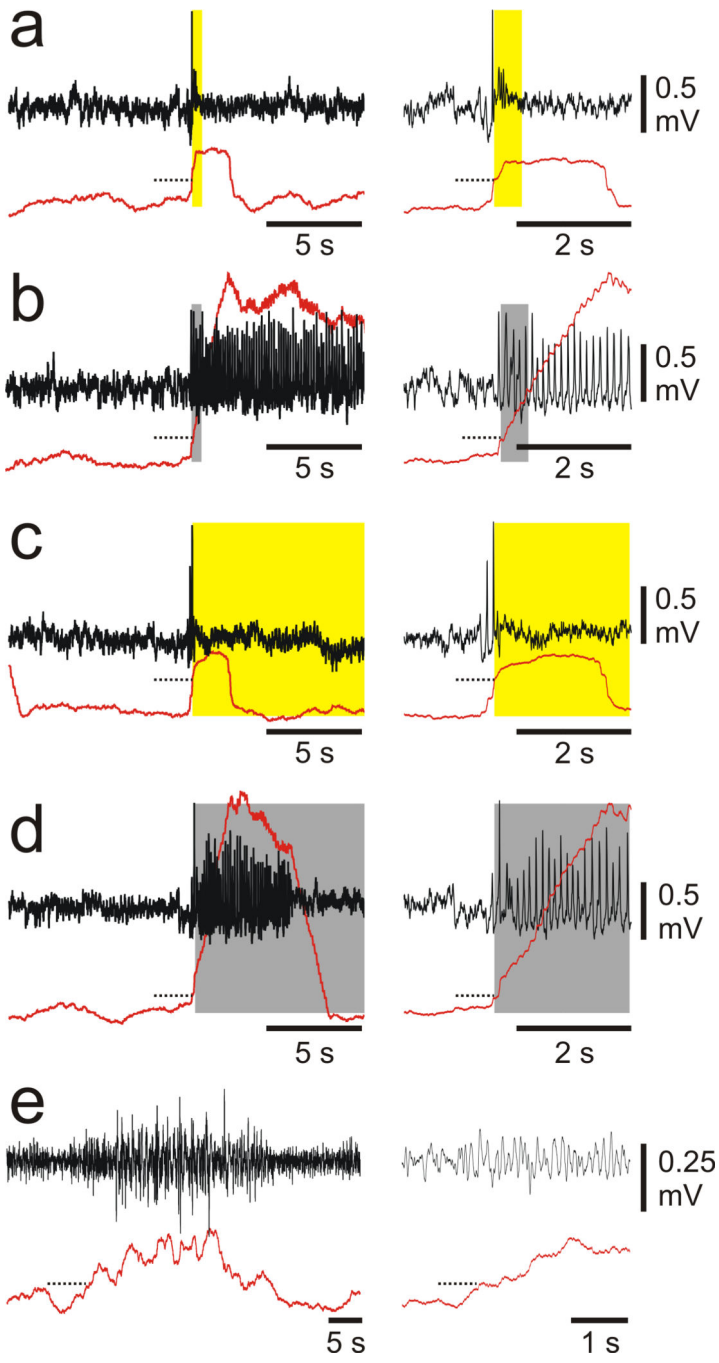

Figure 8. Line-length calculation for real-time detection of seizures

a–e, EEG recordings (Top, black traces) and their corresponding line-length (Bottom red traces) calculated in real-time using a sliding window of 2 s (see Methods for details). Line-length threshold for seizure detection was set manually at the beginning of the experiment. Upon upward crossing of the threshold (dashed line), the system randomly triggered either laser stimulation (yellow boxes) or no stimulation (grey boxes). 0.5 s- and 10 s- long 594 nm

light pulses (10 mW) interrupted the seizure activity in real-time. **a–d** and **e** are from 2 different rats. Traces depicted at the left are enlarged at the right for visibility.